DSPACE

https://dspace.org/

Efficient Adsorption of Lead and Chemical Oxygen Demand from Paint Industry Wastewater by Modified Flamboyant Pods

T.L Adewoye; I.S Fesojaye; Sherif Mustapha; O.A.A Elette; I.A Mohammed ...

https://hdl.handle.net/10539/46087
DOAJ

Downloaded from a DSpace repository. https://dspace.org/

ResearchGate

See discussions, stats, and author profiles for this publication at: https://www.researchgate.net/publication/390448547

Efficient Adsorption of Lead and Chemical Oxygen Demand from Paint Industry Wastewater by Modified Flamboyant Pods

Article *in* Nigerian Journal of Technological Development · February 2025

DOI: 10.4314/njtd.v22i1.3118

CITATIONS
0

READS
79

9 authors, including:



Tunmise Latifat Adewoye
University of Ilorin
18 PUBLICATIONS **236** CITATIONS
SEE PROFILE



Ifeoluwa Sarah Fesojaye
Georgia Institute of Technology
2 PUBLICATIONS **29** CITATIONS
SEE PROFILE



S. I. Mustapha
University of Ilorin
44 PUBLICATIONS **432** CITATIONS
SEE PROFILE



Tosin Oladokun
University of California, Berkeley
1 PUBLICATION **0** CITATIONS
SEE PROFILE

All content following this page was uploaded by Ifeoluwa Sarah Fesojaye on 03 April 2025.

The user has requested enhancement of the downloaded file.

Efficient Adsorption of Lead and Chemical Oxygen Demand from Paint Industry Wastewater by Modified Flamboyant Pods

T. L. Adewoye[1*], I. S. Fesojaye[1], S. I. Mustapha[1,5], O. A. A. Eletta[1], I. A. Mohammed[1], O. O. Oladokun[1], A. S. Abdulkareem[2,4], T. O. Salawudeen[3], O. O. Ogunleye[3]

[1]Department of Chemical Engineering, University of Ilorin, Ilorin, Nigeria.
[2]Department of Chemical Engineering, Federal University of Technology, Minna, Nigeria.
[3]Department of Chemical Engineering, Ladoke Akintola University, Ogbomoso, Nigeria.
[4]Nanotechnology Research Group, Africa Centre of Excellence for Mycotoxin & Food Safety, Federal University of Technology, Minna, Nigeria.
[5]School of Chemical and Metallurgical Engineering, University of the Witwatersrand, South Africa.

ABSTRACT: The removal of heavy metals and organic pollutants from industrial wastewater remains a critical challenge, particularly in the paint industry, where effluents contain high levels of lead (Pb^{2+}) and Chemical Oxygen Demand (COD). This study investigates the adsorption of Pb^{2+} and COD from paint industry wastewater using carbonized Flamboyant Pod Carbon (FPC) and Multi-Walled Carbon Nanotube (MWCNT) modified FPC (FPC/p-MWCNTs) adsorbents. The adsorbents were characterized using Brunauer-Emmett-Teller (BET), X-ray Diffraction (XRD), High-Resolution Scanning Electron Microscopy (HRSEM), and Energy Dispersive Spectroscopy (EDS) to determine their surface area, crystallinity, morphological structure, and elemental properties, respectively. Batch adsorption experiments assessed the effects of contact time, adsorbent dosage, and temperature. Adsorption isotherms and kinetics were also studied. The adsorption process reached equilibrium within 30 minutes for FPC and FPC/p-MWCNTs, whereas pristine MWCNTs required 50 minutes. The maximum adsorption capacities (Q_{max}) of FPC and FPC/p-MWCNTs for Pb^{2+} were 4.08 mg/g and 4.73 mg/g, respectively, while COD adsorption capacities reached 5000 mg/g for both adsorbents. The highest removal efficiencies recorded at optimal conditions (50°C, 0.16 g adsorbent dosage) were 92.5 and 92.06% for Pb^{2+} and COD using FPC, and 93 and 92.61% using FPC/p-MWCNTs, respectively. Adsorption isotherms studies revealed that Pb^{2+} adsorption followed the Freundlich model, indicating multilayer adsorption, while COD adsorption conformed to the Langmuir model, suggesting monolayer adsorption. The kinetic data were best fitted to pseudo-second-order model, and thermodynamic analysis indicated that the adsorption process was endothermic and spontaneous. These findings demonstrate the potential of both FPC and FPC/p-MWCNTs as effective and sustainable adsorbents for industrial wastewater treatment.

KEYWORDS: Flamboyant Pod, MWCNTs, Adsorption, COD, Lead, Wastewater

[Received Nov. 24, 2024; Revised Feb. 4, 2025; Accepted Feb. 13, 2025] Print ISSN: 0189-9546 | Online ISSN: 2437-2110

I. INTRODUCTION

Water pollution is a major global and local environmental challenge, primarily driven by the discharge of untreated or inadequately treated industrial wastewater into water bodies (Abbas *et al*., 2016; Eswaran et al., 2024). Among the various pollutants, heavy metals and high organic loads pose significant risks due to their toxicity, persistence, and potential for bioaccumulation. Heavy metals such as cadmium (Cd^{2+}), zinc (Zn^{2+}), copper (Cu^{2+}), nickel (Ni^{2+}), lead (Pb^{2+}), mercury (Hg^{2+}), and chromium (Cr^{6+}) are commonly found in industrial effluents, originating from activities such as metal plating, mining, smelting, battery manufacturing, tanneries, glass production, petroleum refining, and paint manufacturing (Hashem *et al*., 2024).

Among these industries, the paint manufacturing sector generates wastewater that is particularly challenging to treat due to its high concentrations of heavy metals and organic pollutants (Gondal and Hussain, 2007; Sen, 2023). Lead (Pb^{2+}), cadmium (Cd^{2+}), arsenic (As^{3+}), and mercury (Hg^{2+}) are frequently detected in paint industry effluents, posing severe health and environmental risks even at trace levels (Abdel Salam, 2013; Jibril *et al*., 2021). The persistence of these metals in the environment leads to groundwater contamination, bioaccumulation in aquatic organisms, and adverse health effects such as neurological disorders, organ damage, and carcinogenicity (Emenike *et al*., 2022). Regulatory bodies such as the World Health Organization (WHO) and the U.S. Environmental Protection Agency (EPA) have imposed strict discharge limits on heavy metals in wastewater, necessitating the development of effective treatment methods to meet these standards (Acharya *et al*., 2009).

In addition to heavy metals, Chemical Oxygen Demand (COD) is a critical parameter for assessing water pollution, as it indicates the presence of organic contaminants that deplete dissolved oxygen levels in water bodies (Abdalla & Hammam, 2014; Zhao *et al*., 2024). Paint industry wastewater typically exhibits high COD values, ranging from 425 mg/L to 7662.5 mg/L, which can severely impact aquatic ecosystems by promoting eutrophication and reducing biodiversity (Awogbemi & Von Kallon, 2023).

Among the various treatment methods available, adsorption is widely recognized for its simplicity, cost-effectiveness, and efficiency in removing both organic and inorganic pollutants from wastewater (Mustapha et al., 2017; Saini et al., 2024). Low-cost adsorbents derived from agricultural waste have gained considerable attention due to their abundance, renewability, and minimal processing requirements (Moosavi et al., 2020). Several agricultural by-products, including corn cob, wheat bran, loofah sponge, sorghum stalk, sweet potato stalk, watermelon skins, and wheat husk, have been explored as potential adsorbents (Magaji and Saleh, 2021; Gao et al., 2022). However, despite their affordability and availability, many of these materials exhibit low adsorption capacities due to limited surface area and weak binding sites for pollutant removal (Fu and Wang, 2011). Consequently, modification strategies such as chemical activation, carbonization, and nanomaterial incorporation have been employed to enhance their adsorption performance (Crini *et al*., 2019).

One promising approach is the integration of nanomaterials such as carbon nanotubes (CNTs) with biomass-based adsorbents to improve adsorption efficiency (Parlayici et al., 2015; Liu et al., 2022). CNTs, particularly multi-walled carbon nanotubes (MWCNTs), have demonstrated excellent adsorption capacities due to their large surface area, high mechanical strength, and strong affinity for metal ions and organic pollutants (Abdel Salam, 2013; Sadegh, 2016). These exceptional properties of CNTs have facilitated their various applications including water treatment (Alkali & Fatimah, 2023). However, their high production cost has limited large-scale applications. A viable alternative is the modification of low-cost agricultural waste adsorbents with CNTs to enhance pollutant removal while maintaining economic feasibility.

While significant research has been conducted on agricultural waste-derived adsorbents and CNT-based materials, limited studies have explored the modification of Flamboyant Pod Carbon (FPC) with MWCNTs for treating paint industry wastewater. FPC, derived from *Delonix regia* pods, is a promising biomass-based adsorbent with high carbon content and significant potential for heavy metal and COD removal. However, its adsorption efficiency can be further enhanced. Incorporating MWCNTs into FPC (FPC/p-MWCNTs) is expected to improve its adsorption capacity, selectivity, and reusability, making it a more effective and sustainable solution for industrial wastewater treatment. This research addresses this gap by developing and characterizing carbonized Flamboyant Pod Carbon (FPC) and MWCNT-modified FPC (FPC/p-MWCNTs) adsorbents. The adsorption performance of these materials for Pb^{2+} and COD removal from paint industry wastewater under varying operational conditions was investigated and compared. This research contributes to advancing low-cost, sustainable, and environmentally friendly wastewater treatment solutions while offering insights into the potential application of CNT-modified agricultural adsorbents for industrial effluent remediation.

II. METHODOLOGY

A. Materials

Analytical-grade reagents with a purity range of 95–99.9% were used in this study, all of which were purchased from Sigma Aldrich and used without further purification. The MWCNTs utilized were prepared and purified following the method outlined in our previous study (Adewoye et al., 2021). The wastewater sample was collected from a paint company in Ogun State, South-West Nigeria using a sterile plastic container, placed in an ice box. The concentration of Pb (II) ions was determined using Atomic Absorption Spectroscopy (AAS, 240 FS AA Model). Additionally, the sample was analysed for chemical oxygen demand (COD), biochemical oxygen demand (BOD), conductivity, nitrate, nitrite, turbidity, pH, and colour using standard methods from the literature. The sample was then kept in the refrigerator at 4°C before subsequent use.

B. Preparation of Adsorbents

The Flamboyant Pod Carbon (FPC) was prepared from flamboyant pods (FP) taken from a single tree on the main campus of the University of Ilorin. Before use, the seeds were removed from the FP, and the pods were thoroughly washed multiple times with tap water to eliminate any adhered debris. They were then rinsed with distilled water and air-dried for a day before being oven-dried at 105°C for 4 hours (Alade et al., 2012). After drying, the pods were ground into smaller pieces using a mortar and pestle, and further size reduction was achieved with a milling machine. The processed sample was stored in a clean, dry container before carbonization. Then, 5 g of the fine powder was carbonized at 300°C for 1 hour (Aremu et al., 2017) in an electric furnace, and the resulting charred material was allowed to cool to room temperature. The carbonized sample was then washed with distilled water, filtered, and dried at 105°C for 6 hours. Finally, the dried FPC sample was stored in a sterile container for later use.

The modified adsorbent, FPC/p-MWCNTs was synthesized by incorporating p-MWCNTs onto FPC in the ratio of 1:20 (w/w) using the method adopted by Parlayici et al. (2015). Precisely, 9.5 g of FPC was dispersed in 100 mL of analytical-grade ethanol in a beaker and sonicated for 10 minutes to enhance dispersion. Then, 0.5 g of p-MWCNTs (5 wt%) was added to the solution in the beaker, and the content of the beaker was sonicated for another 10 minutes. The mixture was subsequently dried in an oven at 80°C until all the ethanol evaporated. The resulting FPC/p-MWCNTs were stored in an airtight container for further use.

C. Characterisation of the adsorbents

The prepared adsorbents were characterized for their surface area and pore size using BET. The BET analysis was performed using the nitrogen adsorption-desorption method with Nova 4200e-series. A known weight (0.3g) of the sample was placed in the sample cell and degassed under nitrogen gas N_2 at 250 °C for 4 h in a BET degassing station. The sample was weighed again after degassing and the degassed samples were then analysed for physisorption of the adsorbate (nitrogen) by the adsorbent in a liquid nitrogen environment on the surface.

The morphology and elemental composition of the adsorbents were performed by Zeiss Auriga HRSEM equipped with an In-lens standard detector at 30 kV. A small quantity of the adsorbent was spread on a sample holder and sputter coated with Au-Pd using Quorum T15OT for 5 minutes before analysis. The sputter-coated samples were firmly attached to the carbon adhesive tape and analysed using HRSEM coupled with EDS. The microscope was operated with electron high tension (EHT) of 5 kV for imaging.

Crystalline properties were examined using an X-ray diffractometer (Bruker AXS D8) with Cu Kα radiation (λ = 1.5406 Å) and operating at 45 kV and 40 mA. The scanning rate was 1.5º/min, while a step width of 0.05° was used over the 2θ range value of 20 – 80º.

D. Batch adsorption experiments

Batch adsorption experiments were conducted to investigate the effects of contact time (10, 20, 30, 40,50, and 60 minutes), adsorbent dosage (0.04, 0.08, 0.12, 0.16, and 0.2 g), and temperature (30, 35, 40, 45, and 50°C) on the removal efficiency of the prepared adsorbents. The effect of contact time was conducted by adding 0.16 g of adsorbent to a series of 250 mL conical flasks, each containing 100 mL of the paint wastewater sample. The flasks were sealed and placed in a thermostat water bath shaker, operating at a constant speed of 150 rpm and a temperature of 30ºC. At each time interval after shaking, the samples were removed from the shaker and the mixtures were then filtered using Whatman no. 1 filter paper (Adeleye et al., 2016; Mustapha et al., 2017). The residual concentrations of Pb^{2+} in the filtrate were analysed using AAS, while COD was determined using the titration method described by Yao et al. (2015).

The effect of dosage was conducted by adding varying amounts of adsorbents to a series of 250 mL conical flasks, each containing 100 mL of the paint wastewater sample and placed in the water bath shaker at temperature of 30ºC. the mixtures were shaken at 150 rpm for the predetermined times to achieve equilibrium. Also, the effect of temperature was investigated using an adsorbent dosage of 0.16 g per 100 mL of wastewater. The samples were placed in the water bath shaker at various temperature intervals for a predetermined time. The percentage reduction of COD and removal of Pb^{2+} were calculated using the Equation 1,

$$\%Removal = \frac{C_o - C_e}{C_o} \times 100 \quad (1)$$

Where C_o and C_e are the COD/ Pb^{2+} concentrations in the liquid phase before and at equilibrium adsorption experiments (mg/L), respectively.

The adsorption data were calculated by determining the amount of COD or Pb^{2+} adsorbed per gram of adsorbent, denoted as Q_e (mg/g) at equilibrium and Q_t (mg/g) at any time (t). Q_e and Q_t of COD and Pb^{2+}, were calculated using Equations (2) and (3), respectively.

$$Q_e = \frac{(C_o - C_e) \times V}{W} \quad (2)$$

$$Q_t = \frac{(C_o - C_t)\, V}{W} \quad (3)$$

Where C_t is the concentration of the COD/ Pb^{2+} in the paint wastewater sample at adsorption at any time t; V (mL) is the volume of adsorbate solution; and, W (g) is the mass of adsorbent in the solution (g).

E. Adsorption isotherms studies

Adsorption properties and equilibrium data, known as adsorption isotherms, describe the interactions between pollutants and adsorbents (Ituen et al., 2017). These isotherms are crucial for optimizing both the efficiency and application of adsorbents (Taiwo et al., 2024).

To effectively design an adsorption system for the removal of Pb^{2+} and COD from paint wastewater, it is essential to identify the most suitable equilibrium model (Abdel-Rahman, 2016). In this study, the adsorption data were modelled using the Langmuir, Freundlich, and Temkin isotherm models.

The Langmuir model proposes that pollutant removal from the aqueous phase occurs on homogeneous surfaces through monolayer adsorption, with no interactions between the adsorbed molecules. This isotherm is based on three key assumptions: adsorption is limited to a monolayer, all surface sites are uniform and can each accommodate only one adsorbed atom, and the likelihood of a molecule being adsorbed at a given site is independent of the occupancy of neighbouring sites (Abdel-Rahman, 2016; Dada et al., 2016). The linear form of Langmuir isotherm can be represented by the expression given in Equation 4:

$$\frac{1}{Q_e} = \frac{1}{(K_L\, Q_{max})}\frac{1}{C_e} + \frac{1}{Q_{max}} \quad (4)$$

Where, Q_e is the amount of Pb^{2+} /COD adsorbed per specific amount of adsorbent at equilibrium (mg/g), C_e is the equilibrium concentration of Pb^{2+} /COD in the solution (mg/L); Q_{max} is the maximum amount of Pb^{2+} /COD required to form a monolayer or the maximum adsorption capacity corresponding to the complete monolayer coverage (mg/g) and, K_L is the Langmuir constant which is related to the energy of adsorption (L/mg) (Parlayici *et al*., 2015).

The essential features of the Langmuir adsorption isotherm can be used to predict the affinity between the sorbate and the sorbent using the separation factor or dimensionless equilibrium parameter expressed as R_L presented in Equation 5:

$$R_L = \frac{1}{1 + K_L\, C_o} \quad (5)$$

R_L provides important information about the shape of the isotherm and therefore the nature of adsorption. R_L is between 0 and 1 for favourable adsorption, while $R_L > 1$ represents unfavourable adsorption and $R_L = 1$ represents linear adsorption. The adsorption process is irreversible if $R_L = 0$.

Freundlich isotherm is a widely used isotherm for the description of adsorption equilibrium. The linear form of the Freundlich equation is represented by Equation 6:

$$\log Q_e = \log K_F + \frac{1}{n} \log C_e \quad (6)$$

Where K_F is a constant, indicative of the adsorption capacity, and n is the heterogeneity coefficient.

Linear plots of log Q_e versus log C_e allows the estimation of K_F and n as the plot of the log Q_e versus log C_e has a slope with the value of $1/n$ and an intercept with the magnitude of the log K_F. A larger value of n (smaller value of $1/n$) implies a strong interaction between adsorbent and heavy metal while $1/n$ equal to 1 indicates linear adsorption leading to identical adsorption energies for all sites (Adeleye *et al*., 2016). In general, when the K_F value increases, the adsorption capacity of the adsorbent for a given adsorbate increases.

Temkin considered the effects of some indirect adsorbent/adsorbate interactions on adsorption isotherms and suggested that, because of these interactions, the heat of adsorption of all the molecules in the layer would decrease linearly with coverage. The Temkin isotherm has been used in the following linear form presented in Equation 7:

$$Q_e = \frac{RT}{b_T} \ln K_T + \frac{RT}{b_T} \ln C_e \quad (7)$$

Where, K_T (L/g) is the Temkin isotherm constant; b_T is a constant related to the heat of sorption and, R (8.314 J/mol.K) is the gas constant (Adeleye *et al*. 2016).

F. Adsorption Kinetics Studies

The study of adsorption kinetics describes the solute uptake rate, and evidently, this rate controls the residence time of Pb^{2+} and COD uptake at the solid solution interface. Pseudo-first-order, pseudo-second-order, and Elovich kinetic models were used to analyse data obtained from the experiment to study the kinetics, the mechanism of adsorption of Pb^{2+}, and COD adsorption on FPC, p-MWCNTs and FPC/p-MWCNTs adsorbents. The conformity between experimental data and the predicted model values was examined by coefficient of determination (R^2). Lagergren's first-order rate equation is called pseudo-first-order is summarized as given in Equation 8:

$$\frac{dQ_e}{dt} = k_1(Q_e - Q_t) \quad (8)$$

Where Q_e is the adsorption capacity (mg/g) at equilibrium and Q_t is the adsorption capacity (mg/g) of the adsorbent at time t and k_1 (min^{-1}) is the pseudo-first-order rate constant for the adsorption process. Integration of Equation (8) with the boundary conditions as follows: Q_t = 0, at t = 0 and Q_t, at t = t, gives the linear expression in Equation 9:

$$\ln(Q_e - Q_t) = \ln Q_e - k_1 t \quad (9)$$

The slope of the linear plot of the log $(Q_e - Q_t)$ versus t gives the equilibrium adsorption capacity, whereas the intercept of the plot gives the rate constant of the pseudo-first-order equation (Acharya *et al.*, 2009; Emenike *et al*., 2022).

Pseudo-second-order model is derived based on the sorption capacity of the solid phase, expressed as Equation 10:

$$\frac{dQ_t}{d_t} = k_2(Q_e - Q_t)^2 \quad (10)$$

Integration of Equation (10) with the same boundary conditions results in Equation 11

$$\frac{t}{Q_t} = \frac{t}{Q_e} + \frac{1}{k_2 Q_e^2} \quad (11)$$

The pseudo-second-order rate constant, k_2 (g/mg.min) can be determined by plotting t/Q_t against t.

The Elovich equation was developed to describe the kinetics of heterogeneous chemisorption and the equation assumes that the active sites of the adsorbent are heterogeneous or activation energies that vary continuously with surface coverage and are widely used in liquid-solid adsorption (Thajeel, 2013). The linear Elovich equation is given as follows:

$$q_t = \frac{1}{\beta} ln(\alpha\beta) + \frac{1}{\beta} ln(t) \quad (12)$$

Where α is the initial adsorption rate (mg/g.min), and; β is related to the extent of surface coverage and activation energy for chemisorption (g/mg) (Francis and Uchechukwu, 2014). The values of Elovich parameters, α, and β, were determined from the slope and intercept of lines of the plots of Q_t against ln t.

G. Thermodynamic Studies

The thermodynamic parameters reveal important information about the sorption of heavy metal/COD ions onto the surface of the adsorbent. The values of enthalpy (ΔH°), entropy (ΔS°), and Gibbs energy (ΔG°) can be used to predict the nature of the adsorption.

The free energy of adsorption is given by the expression in Equation 12:

$$\Delta G^o = -RT \ln K_T \quad (12)$$

Where R is the gas constant (J/mol.K), T is the temperature (in Kelvin) and; K_T is the distribution coefficient, which is determined as:

$$K_T = (C_o - C_e)/C_e \quad (13)$$

The values of (ΔH°) and (ΔS°) can be determined from the Van't Hoff equation as given in Equation 14:

$$\Delta G = \Delta H - T\Delta S \quad (14)$$

Combining equation (12) and (14) gives Equation (15)

$$\ln K_T = (\Delta S°/R) - (\Delta H°/RT) \quad (15)$$

According to Equation (15), the slope and intercept of the plot of lnK_T versus $\frac{1}{T}$ gives the estimated values of ΔH and, ΔS.

III. RESULTS AND DISCUSSION

A. Characterisation of adsorbents

Brunauer-Emmett-Teller (BET) analysis reveals that both adsorbents possessed high surface areas, suggesting strong potential for effective adsorption of Pb (II) ions and COD. Specifically, the BJH surface area of FPC is 471.27 m^2/g for the FPC/p-MWCNTs, it was noted that the surface area reduced to 464.95 m^2/g with the incorporation of p-MWCNTs on FPC, which posits that micro-pores may have been covered by the p-MWCNTs which aggregate on the surface of the PFC. It can also be observed that the pore size of FPC increased from 2.80 nm to 2.92 nm upon doping with the p-MWCNTs. This

may be a result of p-MWCNTs which aggregate on the surface of FPC and form a small number of mesopores in the FPC/p-MWCNTs adsorbent (Xing et al., 2016), this may have enhanced the adsorption capacity of FPC/p-MWCNTs. Both adsorbents were classified as mesoporous, with pore radii between 2–50 nm (Storck et al., 1998). The higher surface area of FPC suggests its potential as a promising adsorbent in wastewater treatment.

Figure 1 shows the results of the microstructure analysis of the prepared adsorbents. Figures 1a and 1b compare the HRSEM images of FPC and FPC/p-MWCNTs. The HRSEM image of FPC (Figure 1a) reveals particles with irregular, sheet-like morphologies, featuring numerous steps and edges. The HRSEM shows that the surface of FPC contains pores which may provide sites for the adsorption process. The HRSEM micrograph of FPC/p-MWCNTs reveals changes in the surface morphology of FPC/p-MWCNTs with the appearance of heterogeneous particles different from FPC. The HRSEM image of FPC/p-MWCNTs (Figure 1b) clearly shows aggregated spiral-like p-MWCNTs (indicated by arrows) embedded within the sheet-like particle of FPC, confirming the successful incorporation of the p-MWCNTs in the matrix of FPC. This result is in agreement with the findings of Parlayici et al. (2015) and Eswaran et al. (2024). The irregular texture of both adsorbents suggests the presence of numerous binding sites, which could enhance the adsorption efficiency. Additionally, the compact orientation of the p-MWCNTs seen on the matrix of FPC/p-MWCNTs may enhance its adsorption capacity as previously observed by Parlayici et al. (2015) for AC/f-MWCNTs.

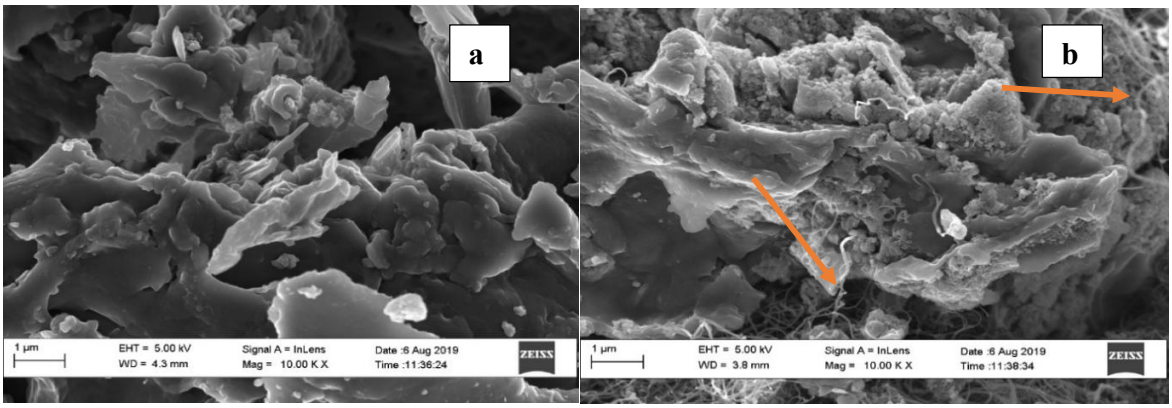


Figure 1: SEM micrograph of the synthesized adsorbents (a) FPC, and (b) FPC/p-MWCNTs

Figure 2 shows the the results of EDS elemental composition analysis of the adsorbents, and the EDS spectra for FPC and FPC/p-MWCNTs are presented in Figures 2a and 2b, respectively. Interestingly, FPC was found to contain 88.54% oxygen, with no detectable carbon. The high oxygen content observed may have contributed to the high adsorption efficiency displayed by the FPC. This result is in contrast with the previous reports by Babalola et al (2020), who reported 57.61 % Carbon and 41.15 % Oxygen, and Okoya et al. (2020) who reported 44.27% carbon and 34.2% oxygen. Also, the EDS reports of Yaumi et al. (2023) reveal a very high percentage of Fe content. The observed difference in the elemental composition of FPC adsorbent in this study and the literature may be linked to the difference in the geographical location where the samples were obtained. Upon incorporation of p-MWCNTs on the matrix of FPC, the percentage of oxygen reduced while carbon became more dominant (80.21%), an indication that the p-MWCNTs were well dispersed on the matrix of FPC corroborating the HRSEM result.

The EDS spectra of both adsorbents indicated the presence of magnesium (Mg), silicon (Si), potassium (K), and calcium (Ca) in both adsorbents. Additionally, trace amounts of zinc (Zn), phosphorus (P), and chlorine (Cl) were identified only in FPC/p-MWCNTs. The presence of aluminum (Al) and silicon (Si) in FPC/p-MWCNTs is likely due to the support used during the synthesis of p-MWCNTs (Adewoye et al., 2021). The presence of other elements, such as oxygen (O), sodium (Na), magnesium (Mg), aluminum (Al), silicon (Si), phosphorus (P), sulphur (S), chlorine (Cl), potassium (K), calcium (Ca), and iron (Fe), may further contribute to enhancing the adsorption process (Okoya et al., 2020).

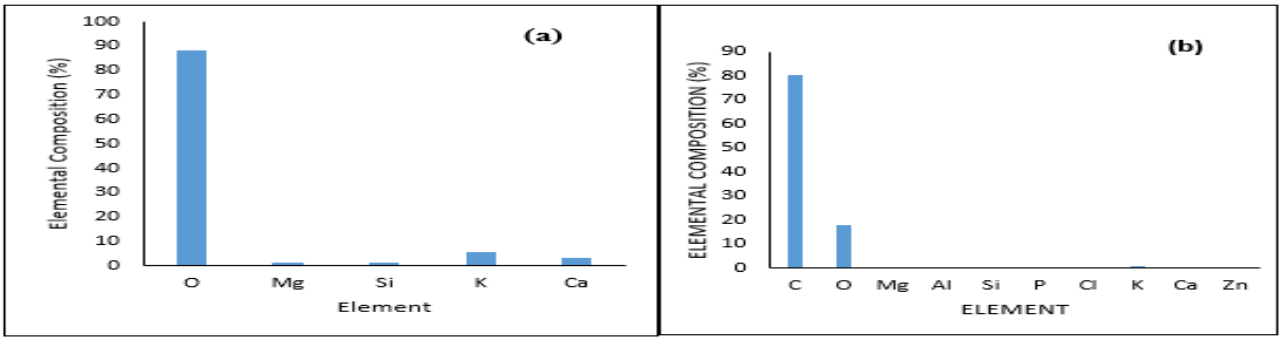


Figure 2: EDS analysis of the elemental composition of the synthesized adsorbents (a) FPC, and (b) FPC/p-MWCNTs

Figure 3 shows the X-ray diffraction (XRD) analysis patterns of (a) p-MWCNTs, (b) FPC, and (c) FPC/p-MWCNTs adsorbents. As shown in Figure 3(a), the XRD patterns of p-MWCNTs reveal the characteristic sharp peaks of graphitized carbon around 2Θ of 26° (002) and 44° (100) similar to the report by Taha et al. (2022) for MWCNTs. The intensity and sharpness of the peaks indicate that the p-MWCNTs are highly crystalline. The XRD patterns of FPC depicted in Figure (3b) show the amorphous nature of the particle probably due to the presence of lignin as previously observed by Abdel-Rahman (2018). The XRD results for FPC are consistent with the findings of Abdel-Rahman (2016) for *Delonix regia* pod powder. Figure 3 (c) displays the XRD patterns FPC/p-MWCNTs, it was observed that the diffraction pattern FPC/p-MWCNTs adsorbent exhibits similar diffraction patterns to that of FPC adsorbent. The characteristic peaks of p-MWCNTs appear to overlap with that of FPC in the diffraction pattern of FPC/p-MWCNTs possibly because of the ratio of quantity of the p-MWCNTs to FPC (1:20 w/w). Nevertheless, the HRSEM and EDS results confirmed the successful incorporation of p-MWCNTs into the matrix of the FPC.

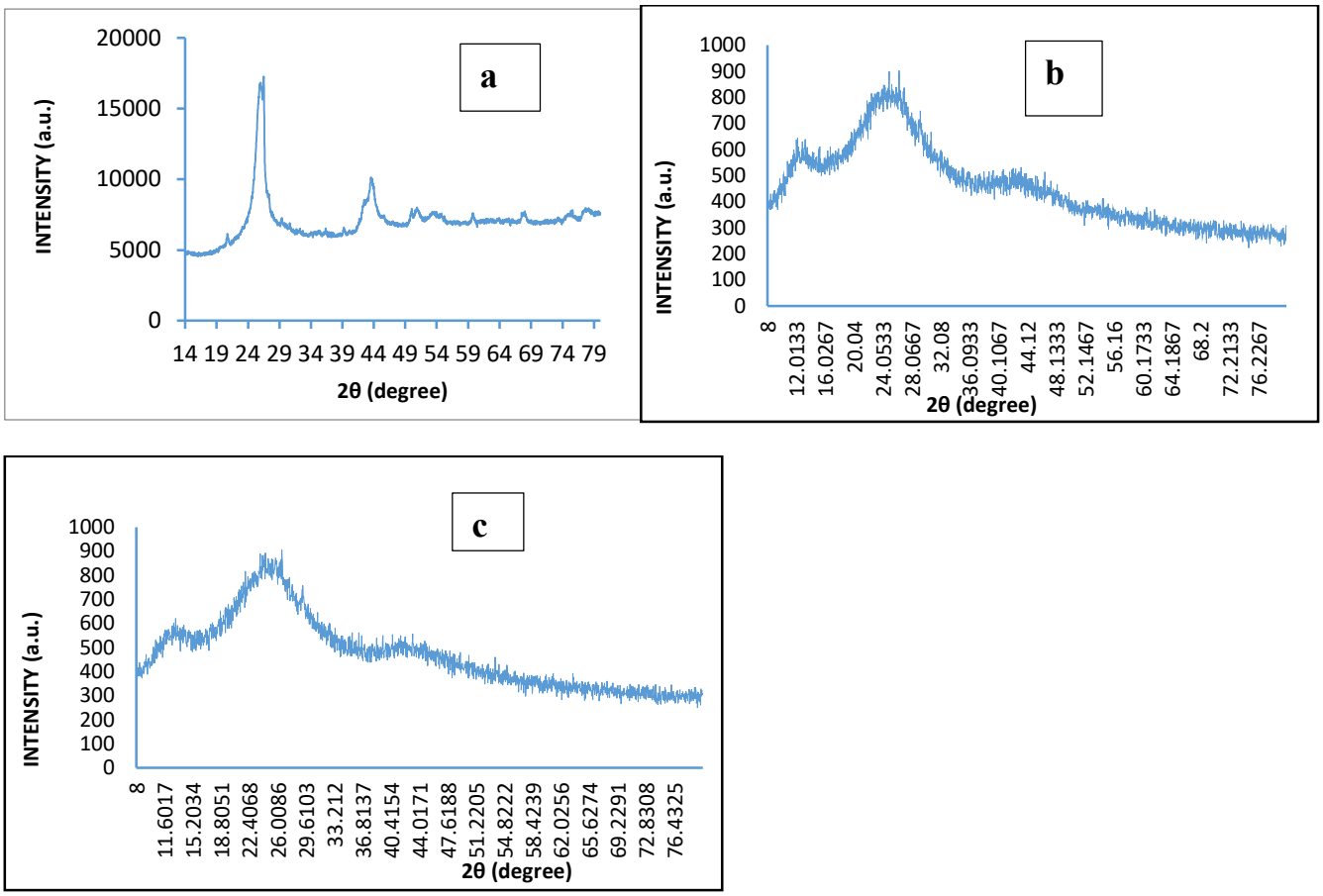


Figure 3: XRD patterns of the synthesized adsorbents (a) p-MWCNTs (b) FPC, and (c) FPC/p-MWCNTs

B. Effect of adsorption parameters

The adsorption of COD and Pb^{2+} is affected by variations in contact time, temperature, and adsorbent dosage. These three parameters were varied for the Pb^{2+} and COD on the three adsorbents (FPC, FPC/p-MWCNTs, and p-MWCNTs for comparison. Figure 4 illustrates the effect of contact time on the adsorption efficiencies of FPC, p-MWCNTs, and FPC/p-MWCNTs for (a) removal of Pb^{2+} and, (b) reduction of COD from paint wastewater, respectively. The rapid adsorption observed in the initial stage is likely due to the high concentration gradient between Pb^{2+} /COD in the solution and the available vacant adsorption sites on the adsorbents. This fast initial uptake could be attributed to the large number of vacant sites available at the beginning of the adsorption process. As time progresses, the rate of adsorption gradually increases until equilibrium is reached. This progressive increase may be due to the limited mass transfer of adsorbate molecules from the bulk liquid to the external surface of the adsorbents, followed by a slower internal mass transfer within the adsorbent particles (Acharya et al., 2009). The subsequent decline in adsorption rate can be attributed to the filling of the pores in the adsorbent with water molecules (Karimi-Maleh et al., 2021), reducing the availability of vacant adsorption sites. This result is consistent with the findings of Yaumi et al., (2023)

From Figure 4a, it is evident that the percentage removal of Pb^{2+} increased with time for both FPC and FPC/p-MWCNTs, reaching equilibrium at 30 minutes, while p-MWCNTs reached equilibrium at 50 minutes. A similar trend was observed for the percentage reduction of COD (Figure 4b) where a sharp decrease in reduction efficiency was noted with a further increase in time. At equilibrium, the removal efficiency for Pb^{2+} was 89.5% for both FPC and FPC/p-MWCNTs, compared to 91.5% for p-MWCNTs. Similarly, the reduction efficiencies for COD were 89.44% and 88.56% for FPC and FPC/p-MWCNTs, respectively, with p-MWCNTs achieving 90%. After equilibrium was reached, the removal efficiency began to decrease slightly until the 60-minute mark. Notably, FPC demonstrated a strong affinity for the pollutants, particularly for COD, where the percentage reduction was marginally higher than that of FPC/p-MWCNTs. Agricultural waste-based adsorbents are often limited by their low adsorption capacity but the PFC adsorbent synthesized in this study has shown a good affinity for the co-sorption of Pb^{2+} and COD from paint effluent. This result is in good agreement with Okoya et al., (2020) for the adsorption of Indigo dye from textile industrial wastewater. This high performance displayed by FPC may be due to the presence of high oxygen content which may serve as the binding site for the pollutants leading to enhanced adsorption efficiency. However, FPC/p-MWCNTs demonstrated a fast initial adsorption rate achieving a reduction percentage of 71.87% within the first ten minutes compared with FCP adsorbent which achieved a reduction efficiency of 66.67% in the first ten minutes. This result suggested that the incorporation of the p-MWCNTs in the matrix of the FPC/p-MWCNTs slightly enhanced the initial adsorption rate of COD as CNTs have great potential as novel adsorbents due to their unique properties. The high affinity of FPC for the pollutants considered in this study may be attributed to its high surface area and elevated oxygen content, as revealed by BET and EDS analyses, respectively. This demonstrated the potential of FPC as an effective sustainable adsorbent for the removal of contaminants from paint industry effluent.

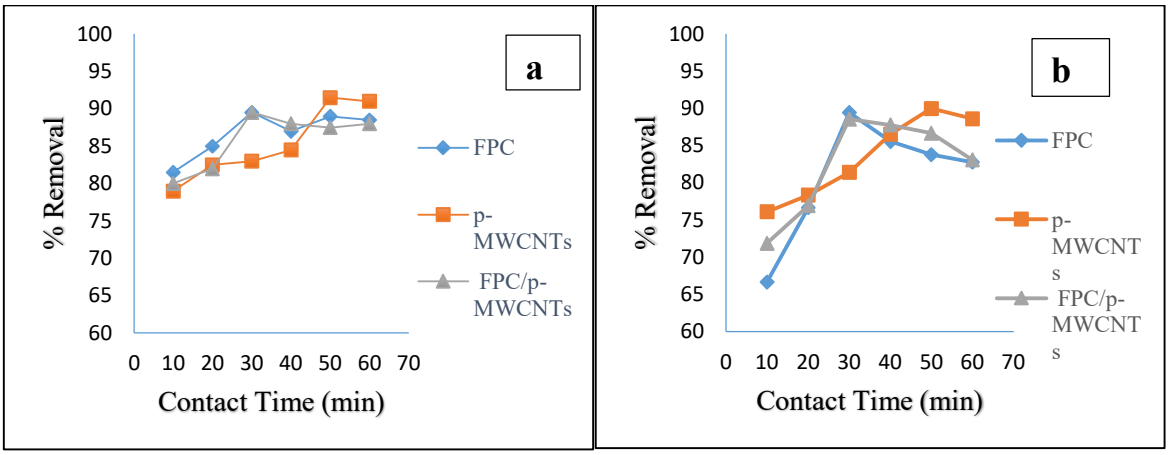


Figure 4: Effect of contact time on the percentage removal/reduction of (a) Pb^{2+} and (b) COD using FPC, p-MWCNTs, and FPC/p-MWCNTs

Adsorbent dosage is a key factor that significantly impacts the adsorption process by influencing the adsorbent's capacity to remove the adsorbate. Figure 5 shows the relationship between contact time and the sorption of (a) Pb^{2+} and (b) COD onto FPC, p-MWCNTs, and FPC/p-MWCNTs at varying adsorbent dosages.

As shown in the figures, the percentage removal of Pb^{2+} and, percentage reduction of COD increased sharply with the rise in adsorbent dosage, but plateaued after a certain point: 0.16 g for both FPC and FPC/p-MWCNTs, and 0.20 g for p-MWCNTs. This stabilization indicates that beyond these dosages, further increases in adsorbent mass did not

significantly enhance removal efficiency. The initial sharp increase in removal can be attributed to the greater availability of sorption sites, as previously reported by Yang et al. (2019). As the adsorbent dosage increases, the available surface area also increases, promoting the adherence of Pb^{2+} and COD onto the adsorbent. The highest removal efficiencies were observed with p-MWCNTs, achieving 92.5% for Pb^{2+} and 90% for COD. Consequently, an adsorbent dose of 0.16 g per 100 mL is deemed optimal for all three adsorbents.

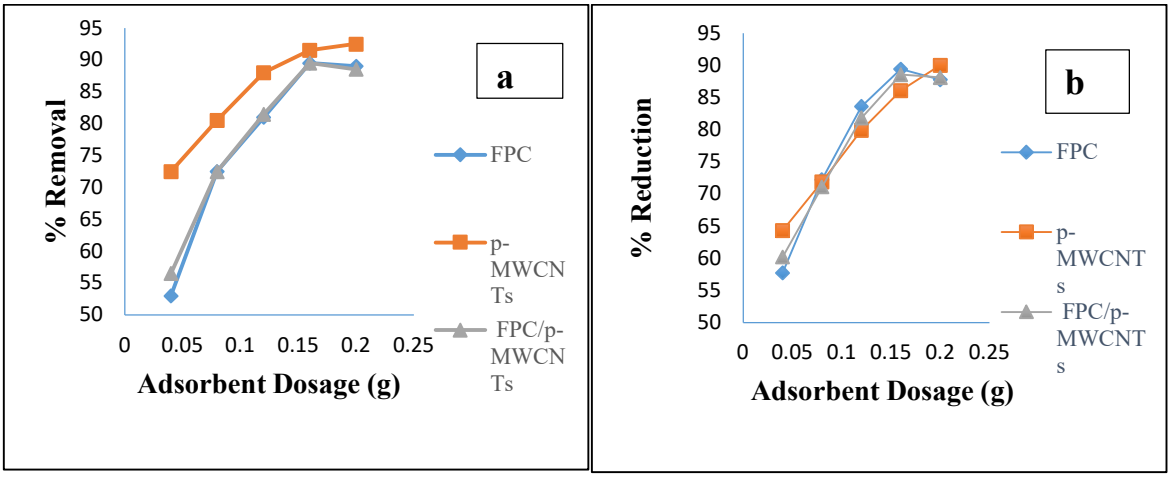


Figure 5: Effect of adsorbent dosage on the percentage removal/reduction of (a) Pb^{2+} and (b) COD using FPC, p-MWCNTs, and FPC/p-MWCNTs

Temperature is another important factor that can significantly impact the removal of Pb^{2+} and, reduction COD from wastewater. Figure 6 shows the effect of temperature on the adsorption of (a) Pb^{2+} and, (b) COD onto FPC, p-MWCNTs, and FPC/p-MWCNTs using an adsorbent dosage of 0.16 g per 100 mL of wastewater, with contact times of 30 minutes for FPC and FPC/p-MWCNTs, and 50 minutes for p-MWCNTs. The results indicate that temperature has a slight but noticeable effect on the adsorption efficiency of all three adsorbents. As seen in Figures 6a and 6b, adsorption efficiency increased marginally with rising temperature, suggesting that the process is endothermic. This can be attributed to the faster diffusion of Pb^{2+} and COD in the solution, likely due to a decrease in solution viscosity at higher temperatures (Abbas et al., 2016). The highest removal efficiencies were observed at 50ºC, with FPC achieving 92.5% Pb^{2+} removal and 92.06% COD reduction, FPC/p-MWCNTs achieving 93% Pb^{2+} removal and 92.61% COD reduction, and p-MWCNTs achieving 94% Pb^{2+} removal and 94.11% COD reduction.

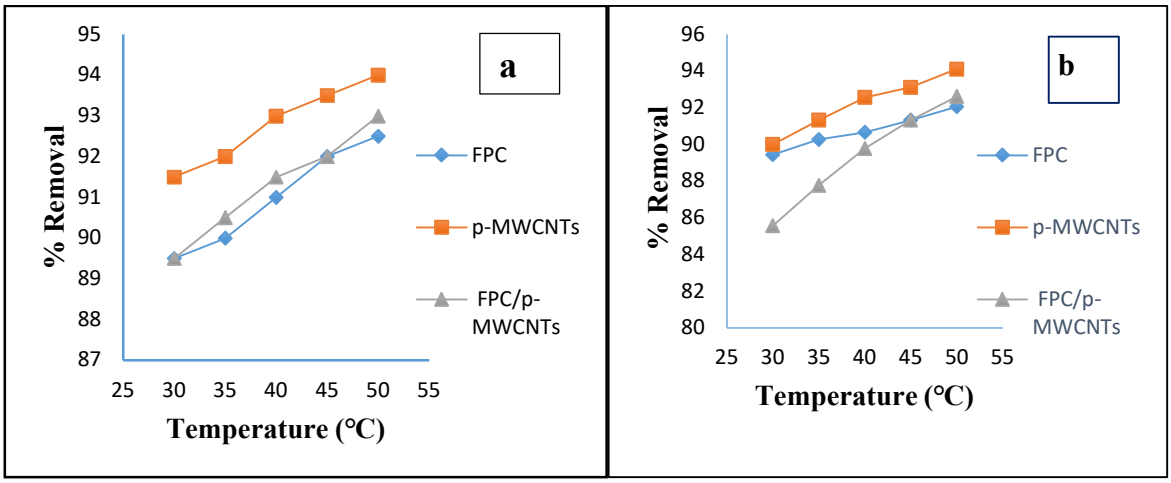


Figure 6: Effect of temperature on the percentage removal/reduction of (a) Pb^{2+} and (b) COD adsorption using FPC, p-MWCNTs and FPC/p-MWCNTs

C. Adsorption Isotherm Model

The Langmuir, Freundlich, and Temkin adsorption isotherm models were applied to analyze the equilibrium data obtained from the adsorption of Pb^{2+} and COD onto FPC, FPC/p-MWCNTs, and p-MWCNTs. This analysis was conducted to understand the interaction between the adsorbents and the adsorbates. Adsorption isotherm parameters were calculated from the linear plots of the Langmuir, Freundlich, and Temkin models (not shown) and are presented together with coefficient of determination (R^2) in Table 1.

The Langmuir isotherm model, with an R^2 value of 0.97, provided the best fit for Pb^{2+} adsorption onto p-MWCNTs, suggesting that the adsorption occurred on homogeneous surfaces (Abbas et al., 2016). Additionally, the separation factor R_L value was calculated to be 0.59, indicating a favorable adsorption process (Dada et al., 2017). Interestingly, Table 1 also shows that both Langmuir and Temkin isotherm models better described the adsorption of COD onto p-MWCNTs. The Temkin model's equilibrium binding constant K_T, which relates to the maximum binding energy, was found to be 0.008, indicating moderately high binding energy of COD onto the p-MWCNTs adsorbent. The adsorption of Pb^{2+} onto FPC and FPC/p-MWCNTs is best fitted to the Freundlich isotherm model suggesting adsorption on heterogeneous surfaces (Kouakou et al., 2022), likely due to the presence of various binding sites on these adsorbents. The values of 1/n, being less than 1, indicated a favorable adsorption process and the potential for chemisorption (Abdel-Rahman, 2016). The predicted adsorption capacities K_F, based on the Freundlich model, were 2.69 and 2.94 L/mg for FPC and FPC/p-MWCNTs, respectively. Additionally, the equilibrium adsorption data for COD onto FPC was best fitted to the Freundlich isotherm model, while for FPC/p-MWCNTs, the Langmuir model provided the best fit.

Table 1: Adsorption isotherm model parameters for Pb^{2+} and COD adsorption on FPC, p-MWCNTs, and FPC/p-MWCNTs

Isotherms	**Langmuir**				**Freundlich**			**Temkin**		
	Q_{max} (mg/g)	**R_L**	**K_L**	**R^2**	**K_F (L/mg)**	**1/n**	**R^2**	**b_T (J/mol)**	**K_T (L/g)**	**R^2**
Pb^{2+}										
FPC	4.08	0.25	1.48	0.88	2.69	0.65	0.95	2365.6	11.13	0.94
p-MWCNTs	19.31	0.59	0.35	0.97	5.75	0.95	0.96	2060.0	9.59	0.88
FPC/p-MWCNTs	4.73	0.29	1.20	0.85	2.94	0.73	0.93	1366.4	10.20	0.86
COD										
FPC	5000	0.34	0.00110	0.81	16.33	0.75	0.91	2.16	0.01	0.90
p-MWCNTs	5000	0.36	0.00098	0.92	6.09	0.90	0.92	1.76	0.008	0.91
FPC/p-MWCNTs	5000	0.36	0.00097	0.88	10.15	0.92	0.83	1.96	0.008	0.86

D. Adsorption Kinetics Studies

The study of adsorption kinetics helps to describe the rate at which contaminants are absorbed and directly influences the residence time of COD and Pb^{2+} at the solid-solution interface. In this study, pseudo-first-order, pseudo-second-order, and Elovich kinetic models were applied to the data obtained from the kinetic experiments to understand the rate and mechanism of Pb^{2+} and COD adsorption onto FPC, p-MWCNTs, and FPC/p-MWCNTs. The rate constants were calculated from the linear plots (not shown) from kinetic models are summarized in Table 2. The goodness of fit for each kinetic model was evaluated using the coefficient of determination (R^2) values. The results demonstrated that the R^2 values for the pseudo-second-order model were notably high indicating that the adsorption of Pb^{2+} and COD onto the three adsorbents are best described by the pseudo-second-order model suggesting that the adsorption process is primarily governed by a chemical reaction between the metal ions/COD and the active sites on the adsorbent surface (Babalola et al., 2020).

Table 2: Kinetics model parameters for Pb^{2+} and COD adsorption on FPC, p-MWCNTs, and FPC/p-MWCNTs

Adsorbent	**Pseudo-first-order parameters**			**Pseudo-second-order parameters**			**Elovich Parameters**		
	Q_e **(mg/g)**	k_1 **(min^{-1})**	R^2	Q_e **(mg/g)**	k_1 **(min^{-1})**	R^2	**A**	**β**	R^2
Pb^{2+}									
FPC	1.05	0.0545	0.5665	4.5106	0.2287	0.9994	$1.2 * 10^7$	4.9261	0.7800
p-MWCNTs	1.28	0.0397	0.3263	4.7461	0.0676	0.9956	3129.025	2.9386	0.8178
FPC/p-MWCNTs	1.04	0.0451	0.5831	4.5025	0.1843	0.9990	252517.7	4.0145	0.7333
COD									
FPC	198.58	0.0980	0.0053	3333	0.0030	0.9918	56881	0.00227	0.6418
p-MWCNTs	1257.90	0.0490	0.9564	5000	0.00005	0.9975	336070	0.00272	0.8983
FPC/p-MWCNTs	171.14	0.0213	0.0266	3333	0.00023	0.9932	295900	0.00272	0.6502

E. *Thermodynamic Studies*

The effect of temperature on the adsorption process was studied within the range of 30 to 50°C to evaluate thermodynamic parameters, including Gibb's free energy change (ΔG), entropy change (ΔS), and enthalpy change (ΔH). The values of ΔH° and ΔS° were calculated from the slope and intercept of the linear plot of K_T against 1/T (not shown). These thermodynamic parameters, along with the corresponding ΔG° values for the adsorption of Pb (II) ions and COD, are are presented in this section. The presented in Table 3. The results show that the adsorption capacities of the three adsorbents increased with rising temperature for both Pb^{2+} and COD, indicating that the sorption process was endothermic, as evidenced by the positive ΔH° values. This suggests that adsorption efficiency improves with temperature, likely involving a chemisorption mechanism. Additionally, the negative ΔG° values demonstrate the spontaneous and thermodynamically feasible nature of the adsorption process (Acharya et al., 2009).

Table 3: Summary of Thermodynamic studies parameters for Pb^{2+} and COD Adsorption on FPC, p-MWCNTs, and FPC/p-MWCNTs

Temperature	**30** ℃	**35** ℃	**40** ℃	**45** ℃	**50** ℃
Pb^{2+}	**ΔG** ° (J/ mol. K)				
FPC($\Delta H° = 240.30, \Delta S° = 25.51$)	-7488.69	-7616.23	-7743.77	-7871.31	-7998.85
p-MWCNTs ($\Delta H° = 240.29, \Delta S° = 27.53$)	-8100.60	-8238.24	-8375.88	-8513.52	-8651.16
FPC/p-MWCNTs ($\Delta H° = 264.83, \Delta S° = 26.46$)	-7753.86	-7886.18	-8018.50	-8150.82	-8283.14
COD					
FPC ($\Delta H° = 184.18, \Delta S° = 23.79$)	-7022.83	-7141.75	-7260.68	-7379.61	-7498.54
p-MWCNTs ($\Delta H° = 346.21, \Delta S° = 29.64$)	-8634.53	-8782.72	-8930.92	-9079.12	-9227.31
FPC/p-MWCNTs ($\Delta H° = 465.14, \Delta S° = 29.98$)	-8618.80	-8768.70	-8918.60	-9068.50	-9218.40

The units of ΔH° and ΔS° are in J/mol.K

III. CONCLUSION

This study revealed that both FPC and FPC/p-MWCNTs adsorbents demonstrated good potential for effective sorption of Pb^{2+} and COD from paint industry wastewater. The highest removal efficiencies recorded at optimal conditions (50°C, 0.16 g adsorbent dosage) were 92.5% and 92.06% for Pb^{2+} and COD using FPC, and 93% and 92.61% using FPC/p-MWCNTs, respectively. The adsorption process was influenced by contact time, adsorbent dosage, and solution temperature, with adsorbent dosage having the most significant effect. Freundlich isotherm model best described the Pb^{2+} adsorption onto FPC and FPC/p-MWCNTs, indicating multilayer adsorption, while COD adsorption onto FPC/p-MWCNTs conformed to the Langmuir model, suggesting monolayer adsorption, and Freundlich isotherm model best described adsorption of COD onto FPC. The adsorption kinetics was best described by pseudo-second-order model, and thermodynamic analysis indicated that the adsorption process is endothermic and spontaneous. Future research should focus on the performance evaluation of FPC and FPC/p-MWCNTs on effluents from other industries and studies should be extended to column adsorption to provide valuable insight on the performance of the adsorbent under continuous operation to assist in scalability.

AUTHOR CONTRIBUTIONS

T. L. Adewoye: Conceptualization, Methodology, Supervision, Writing – review & editing. **I. S. Fesojaye and O. O. Oladokum:** Methodology, Investigation, Writing – original draft. **S. I. Mustapha, O. A.A. and Eletta:** Conceptualization, Writing – review & editing. **I. A. Mohammed:** Conceptualization, Methodology, Supervision. **O. O. Ogunleye, A. S. Abdulkareem and T. O. Salawudeen:** Conceptualization, Methodology, Supervision.

REFERENCES

Abbas, A., Al-Amer, A. M., Laoui, T., Al-Marri, M. J., Nasser, M. S., Khraisheh, M., & Atieh M. A. (2016). Heavy metal removal from aqueous solution by advanced carbon nanotubes: a critical review of adsorption applications. *Separation and Purification Technology, 157*, 141-161.

Abdalla, K. Z., & Hammam, G. (2014). Correlation between biochemical oxygen demand and chemical oxygen demand for various wastewater treatment plants in Egypt to obtain the biodegradability indices. International Journal of Sciences: *Basic and Applied Research, 13(1)*, 42-48.

Abdel-Rahman, L., Al-Farhan, B., Abu-Dief, A., & Zikry, M. (2016). Removal of toxic Pb (II) ions from aqueous solution by nano sized flamboyant pod (Delonix regia). *Archieve in Chemical Research, 1(1)*, 1-10.

Abdel-Rahman L. H., Abu-Dief A. M., Abd-El Sayed M. A. & M. M. Zikry (2018). Disposal of Heavy Transition Cd^{+2} from Aqueous Solution utilizing Nanosized Flamboyant Pod (Delonix regia). *Journal of Transition Metal Complexes*, *1(2018),*1-10

Abdel Salam, M. (2013). Removal of heavy metal ions from aqueous solutions with multi-walled carbon nanotubes: kinetic and thermodynamic studies. *International Journal of Environmental Science and Technology, 10*, 677-688.

Acharya, J., Sahu, J. N., Mohanty, C. R., & Meikap, B. C. (2009). Removal of lead (II) from wastewater by activated carbon developed from Tamarind wood by zinc chloride activation. *Chemical Engineering Journal, 149(1-3)*, 249-262.

Adeleye, A. S., Conway, J. R., Garner, K., Huang, Y., Su, Y., & Keller, A. A. (2016). Engineered nanomaterials for water treatment and remediation: Costs, benefits, and applicability. *Chemical Engineering Journal, 286*, 640-662.

Adewoye, T., Ogunleye, O., Abdulkareem, A., Salawudeen, T., & Tijani, J. (2021). Optimization of the adsorption of total organic carbon from produced water using functionalized multi-walled carbon nanotubes. *Heliyon, 7(1),* e05866.

Alade, O. A., Amuda, O. O., Ogunleye, O. O., & Okoya, A. A. (2012). Evaluation of Interaction of Carbonization Temperatures and Concentrations on the Adsorption Capacities and Removal Efficiencies of Activated Carbons Using Response Surface Methodology (RSM). *Journal Bioremediation & Biodegradation. 3(1)*, 1–8.

Alkali, M. I., & Fatimah, M. M. (2023). Functionalization and Characterization of Multiwalled Carbon Nanotubes (MWCNTS). *Journal of Basic Physical Research*, *11*(2), 48-57.

Aremu, M., Alade, A., Araromi, D., & Bello, A. (2017). Optimization of process parameters for the carbonization of flamboyant pod bark (Delonix regia). *European Science Journal, 13(24)*, 165-175.

Awogbemi, O., & Von Kallon, D. V. (2023). Progress in agricultural waste derived biochar as adsorbents for wastewater treatment. *Applied Surface Science Advances, 18*, 100518.

Babalola, B. M., Babalola, A. O., Akintayo, C. O., Lawal, O. S., Abimbade, S. F., Oseghe, E. O., Akinola, L. S. & Ayanda, O. S. (2020). Adsorption and desorption studies of Delonix regia pods and leaves: removal and recovery of Ni (II) and Cu (II) ions from aqueous solution. *Drinking Water Engineering and Science*, *13*(2), 15-27.

Crini, G.; Lichtfouse, E.; Wilson, L. D. and Morin-Crini, N. (2019). Conventional and non conventional adsorbents for wastewater treatment. *Environmental Chemistry Letters, 17*, 195-213.

Dada, A. O., Adekola, F. A., & Odebunmi, E. O. (2017). Kinetics, mechanism, isotherm and thermodynamic studies of liquid phase adsorption of Pb^{2+} onto wood activated carbon supported zerovalent iron (WAC-ZVI) nanocomposite. *Cogent Chemistry, 3(1)*, 1351653.

Dada, A. O., Latona, D. F., Ojediran, O. J., & Nath, O. O. (2016). Adsorption of Cu (II) onto bamboo supported manganese (BS-Mn) nanocomposite: effect of operational parameters, kinetic, isotherms, and thermodynamic studies. *Journal of Applied Sciences and Environmental Management, 20(2),* 409-422.

Deyi, A. V., Yaumi, A. L., Umar, H., Aji, M. M., & Mustafa, B. G. (2023). Adsorptive properties of Flamboyant seed pod activated carbon for the removal of anionic dye in wastewater. *Arid Zone Journal of Basic and Applied Research 2(5)*, 124-131.

Emenike, E. C., Ogunniyi, S., Ighalo, J. O., Iwuozor, K. O., Okoro, H. K., & Adeniyi, A. G. (2022). *Delonix regia* biochar potential in removing phenol from industrial wastewater. *Bioresource Technology Reports, 19*, 101195.

Eswaran, P., Madasamy, P. D., Pillay, K., & Brink, H. (2024). Sunlight-driven photocatalytic degradation of methylene blue using ZnO/biochar nanocomposite derived from banana peels. *Biomass Conversion and Biorefinery*, 1-21.

Francis, O. K., & Uchechukwu, S. C. (2014). Adsorption kinetics of Ni (II) and Pb (II) ions from aqueous solutions by husks of Irvingia gabonensis. *International Journal of Chemical Science, 12(4),* 1395-1405.

Fu, F., & Wang, Q. (2011). Removal of heavy metal ions from wastewaters: a review. *Journal of environmental management, 92(3)*, 407-418.

Gao, S., Gong, W., Zhang, K., Li, Z., Wang, G., Yu, E., Xia Y., Tian J., Li H., & Xie, J. (2022). Effectiveness of agricultural waste in the enhancement of biological denitrification of aquaculture wastewater. *Peer-Reviewew Scientific Journal, 10*, e13339.

Gondal, M., & Hussain, T. (2007). Determination of poisonous metals in wastewater collected from paint manufacturing plant using laser-induced breakdown spectroscopy. *Talanta, 71(1)*, 73-80.

Hashem, M. A., Nayeen, J., Hossain, M. T., & Miem, M. M. (2024). Chromium adsorption on thermally activated adsorbent equipped from waste biomass. *Waste Management Bulletin 2 (1),*239-249.

Ituen, E., Akaranta, O., & James, A. (2017). Evaluation of performance of corrosion inhibitors using adsorption isotherm models: an overview. *Chemical Science International Journal, 18(1),* 1-34.

Jibril, H. B., Salga, S. M., Ahmed, S., & Saddiq, M. (2021). Application of agricultural wastes for the aqueous removal of heavy metals from waste water. *Fudma Journal of Sciences, 5(3),* 231-236.

Karimi-Maleh, H., Ayati, A., Ghanbari, S.; Orooji, Y., Tanhaei, B., Karimi, F., Alizadeh M., Rouhi J., Fu L., & Sillanpää, M. (2021). Recent advances in removal techniques of Cr (VI) toxic ion from aqueous solution: A comprehensive review. *Journal of molecular liquids, 329*, 115062.

Kouakou, Y. U., Abo, E. A., Yobouet, Y. A., & Trokourey, A. (2022). Kinetic and thermodynamic study of the adsorption of methylene blue on activated carbon based on corn cobs. *Journal of Materials and Environmental Science*, *13*(4), 367-381.

Liu, G., Dai, Z., Liu, X., Dahlgren, R. A., & Xu, J. (2022). Modification of agricultural wastes to improve sorption capacities for pollutant removal from water–a review. *Carbon Research, 1(1),* 24.

Magaji, M., & Saleh, M. (2021). Aqueous phase removal of heavy metals from contaminated wastewater using agricultural wastes. *ChemSearch Journal, 12(1),* 153-161.

Moosavi, S., Lai, C. W., Gan, S., Zamiri, G., Akbarzadeh Pivehzhani, O., & Johan, M. R. (2020). Application of efficient magnetic particles and activated carbon for dye removal from wastewater. *ACS omega, 5(33),* 20684-20697.

Mustapha, S. I., Adewoye, L. T., Aderibigbe, F. A., Alhaji, M. H., Adekola, M. I., & Tijani, I. A. (2017). Removal of Lead and Chromium from Aqueous Solution onto Flamboyant (*Delonix regia*) Pod Activated Carbon. *Nigerian Journal of Technological Development, 14(2),* 56-66,

Okoya, A. A., Diisu, D. O., Olaiya, O. O., & Sherifdeen, O. (2020). Adsorption Efficiency of Flamboyant Pods for Indigo Dye Removal from Textile Industrial Wastewater. *Environment and Pollution, 9(2),* 1-13.

Parlayici, S., Eskizeybek, V., Avcı, A., & Pehlivan, E. (2015). Removal of chromium (VI) using activated carbon-supported-functionalized carbon nanotubes. *Journal of Nanostructure in Chemistry 5(3),* 255-263.

Sadegh, H.; Shahryari, G. R..; Masjedi, A.; Mahmoodi, Z. and Kazemi, M. (2016). A reviewon Carbon nanotubes adsorbents for the removal of pollutants from aqueous solutions. *International Journal of Nano Dimension., 7 (2),* 109-120.

Saini, K., Singh, J., Malik, S., Saharan, Y., Goyat, R., Umar, A., Akbar, S., Ibrahim, A. A., & Baskoutas, S. (2024). Metal-Organic Frameworks: A promising solution for efficient removal of heavy metal ions and organic pollutants from industrial wastewater. *Journal of Molecular Liquids 399,* 124365.

Sen, T. K. (2023). Agricultural solid wastes based adsorbent materials in the remediation of heavy metal ions from water and wastewater by adsorption: a review. *Molecules, 28(14),* 5575.

Storck, S.; Bretinger, H. and Maier, W. F. (1998). Characterization of micro-and mesoporous solids by physisorption methods and pore-size analysis. Applied Catalysis A: *General, 174(1-2),* 137-146.

Taha, W. M., Morsy, M., Nada, N. A., & Ibrahim, M. A. (2022). Preparation and Characterization of Multiwall Carbon Nanotubes Decorated with Coper Oxide. *Egyptian Journal of Chemistry*, *65*(7), 305-312.

Taiwo, A. E., Musonge, P., & Jegede, O. D. (2024). Bioprocessing of Industrial Wastewater for Removal of Heavy Metal Ion by Ulva Lactuca (Seaweed) Biomass. *Chemical Engineering Transactions*, *109*, 475-480.

Thajeel, A. S. (2013). Isotherm, Kinetic, and Thermodynamic of Adsorption of Heavy Metal Ions onto Local Activated Carbon. *Aquatic Science and Technology*, *1*(2), 53–77.

Xing, B., Shi, C., Zhang, C., Yi, G., Chen, L., Guo, H., Huang G. & Cao, J. (2016). Preparation of TiO_2/activated carbon composites for photocatalytic degradation of RhB under UV light irradiation. *Journal of nanomaterials, 2016*(1), 8393648.

Yang, J., Hou, B., Wang, J., Tian, B., Bi, J., Wang, N., Li X., & Huang, X. (2019). Nanomaterials for the removal of heavy metals from wastewater. *Nanomaterials, 9(3),* 424.

Yao, N., Liu, Z., Chen, Y., Zhou, Y., & Xie, B. (2015). A novel thermal sensor for the sensitive measurement of chemical oxygen demand. *Sensors, 15(8),* 20501-20510.

Zhao, D., Lu, H., Liu, H., Zhang, B., Chen, Q., Yan, Q., Gu, X., Yuan, B., Al-Farraj, S., Nguyen, K. & Sillanpää, M. (2024). A Laboratory Investigation of the Adsorption Performance and Mechanism of Organics in Industrial Wastewater on mp-Zr (OH) 4. *Journal of Water Process Engineering, 61*, 105327.

View publication stats